Proceedings of GT2005
ASME Turbo Expo 2005: Power for Land, Sea and Air
June 6-9, 2005, Reno-Tahoe, Nevada, USA

DRAFT

GT2005-68284

NUMERICAL MODELING OF FLOW AND THERMAL PATTERNS WITHIN A COMBUSTOR SIMULATOR

V. R. Kunze and M. Wolff
Department of Mechanical & Materials Engineering
Wright State University
Dayton, OH, 45435

M. D. Barringer and K. A. Thole
Department of Mechanical Engineering
Virginia Polytechnic Institute and State University
Blacksburg, VA, 24060

M. D. Polanka
Air Force Research Laboratory
Wright-Patterson Air Force Base, OH, 45433

ABSTRACT

Performance enhancements and control of heat transfer in high pressure gas turbine vanes and rotors is dependent on understanding the flow and thermal fields approaching the turbine. The flow field exiting the combustor has highly non-uniform pressure and temperature variations in both the radial and circumferential directions as well as high turbulence levels. Several studies have shown significant impact on the overall and secondary flow fields within the turbine due to the inlet profile. The Turbine Research Facility (TRF) at Wright-Patterson Air Force Base has recently added a non-reactive full scale annular combustor simulator to the facility to study these effects.

In conjunction with the TRF's experimental efforts to simulate combustor section exit flows, a three-dimensional CFD analysis of the newly installed simulator has been undertaken. The analysis aids in the experimental implementation of the simulator and gives further understanding of the simulator's complex internal flow patterns. The goals for the TRF's simulator's is to produce a wide range of profiles to the inlet plane of the vane for evaluation of effects on heat transfer, loss, and loading. The CFD analysis allows an understanding of how those profiles are obtained by tracking the flow through two rows of staggered dilution holes and six rows of staggered film cooling holes on both the ID and OD liners of the main simulator chamber. This enables control as the CFD can guide the experimenter in knowing which liner component influenced the turbine inlet profile shape. Cases can then be run computationally by varying the mass flows and temperatures to tailor the profile to the desired shape prior to running the experiment. These profiles can then be sent through the turbine stage both computationally and experimentally to understand their impact. Finally, turbine airfoils and cooling patterns can then be designed to take advantage of this knowledge.

NOMENCLATURE

C_p	[1]	normalized total pressure $C_P = \frac{P_0 - P_{0,ms-ave}}{0.5\rho_{ave}U_{ave}^2}$
D	[-]	dilution jet
FC	[-]	film cooling jet
I	[1]	momentum flux ratio $I = \frac{\rho_j U_j^2}{\rho_\infty U_\infty^2}$
k	[m^2/s^2]	turbulent kinetic energy
L	[m]	simulator axial length
$\dot{m}$	[kg/s]	mass flow rate
S	[m]	simulator exit span
TU	[1]	turbulence intensity $TU = \frac{\sqrt{2 \cdot k}}{U_{ave}}$
U	[m/s]	velocity magnitude $U = \sqrt{u^2 + v^2 + w^2}$
V	[1]	normalized velocity magnitude $V = \frac{U}{V_{\max}}$
u,v,w	[m/s]	mean velocity components
X,R,Φ	[-]	simulator coordinate system
ε	[m^2/s^3]	dissipation rate of k
Θ	[1]	normalized temperature $\Theta = \frac{T - T_{ave}}{T_{ave}}$

Subscripts

∞	freestream
1,2	dilution jet row
0	total conditions
ave	average
ms-ave	mid span average
ID, OD	inner/outer diameter

INTRODUCTION

The performance of the turbine stage is highly dependent on the approaching upstream flowfield, which requires engineers to study the interaction between the combustor and the downstream turbine stage. Many turbine designs are based on the assumption of a standard turbulent boundary layer inlet profile. However, gas-turbine combustors have highly complex internal flow fields that generate radial and circumferential variations in total pressure, total temperature, and turbulence intensity. It has therefore become increasingly important to understand and characterize the flow within the combustor section of the engine in order to design high performance turbine stages. The Turbine Research Facility has recently completed the installation of a full scale annular combustor simulator. This new capability enables a quantitative experimental study of various combustor exit profiles and their effect on turbine performance. In order to characterize and further understand the complex experimental flowfield exiting the combustor simulator a fully three-dimensional steady-state, computational fluid dynamic (CFD) analysis has been performed using the commercially available CFD code Star-CD™.

CFD predictions are an important tool in directing the experimental settings used to generate the desired spanwise and pitchwise variations in the simulator exit plane. A CFD analysis predicts the entire internal combustor flowfield whereas only a discrete set of data points are gathered with an experimental test run. Thus the CFD analysis helps to understand a broader spatial range of the internal flow field which dictates how the resultant profiles are generated. Once validated against the first series of experimental results the computational database will be used to forecast the exit field profiles, which will enable the inlet condition for the turbine to be properly set.

Many studies have been performed on reacting and non-reacting combustors producing similar turbulence levels regardless of reaction Bicen [1]. The key to simulating this environment is simulating the combustor flowfield by injection of secondary flow through dilution holes, film cooling holes, and slots. This is the methodology Barringer et al. [2] employed in designing and building this simulator.

Previous work relevant to this analysis includes both computational and experimental studies, including studies in fluid dynamic areas relevant to combustor research such as transverse jets and impinging jets in crossflow. Fernandes et al. [3] experimentally studied opposed round jets in confined and unconfined channel cross flows using a two-component laser-Doppler anemometer. Channeled flow and impinging flow regimes were characterized with respect to high (155) and low (60) momentum flux ratios. Opposed jets of the channeled flow regime gradually merge and resemble a single co-flowing jet downstream of their injection point and pinch off regions of the crossflow where they merge. Impinging jets exhibit modest bending and produce counter rotating vortices approximately 2.5 jet diameters upstream of the impingement region.

Khan and Johnston [4], Küpper and Henry [5], Morton and Ibbetson [6], and Sgarzi and Leboeuf [7] are among many notable researchers to investigate jet injection in a crossflow for various angles of injection and velocity ratios. Using both experimental and numerical methods of investigation, the universal significant findings are the confirmation of the embedded vortex pair in the transverse jet and the deflected boundary layer surrounding the jet. Numerical studies using the standard k-ε turbulence model tend to under predict the mixing of the jet with the cross flow, but the depth of jet penetration into the cross flow fluid can be accurately predicted. This is apparent through sharp points in the profiles.

Many experimental and computational studies have focused on injection of film cooling flow. Bazdidi-Tehrani et al. [8] used both the standard and RNG k-ε turbulence models to study coolant jets for a momentum flux range of 6.0-23.5, duct height to jet diameter ratio range of 4.0-12.0, and adjacent jet spacing to jet diameter ratios within the range of 2.0-4.0, which are concurrent with the range of this study. The accuracy of the turbulence models depended on the momentum flux ratio of the jets. The RNG and standard k-ε models performed equally well below a momentum flux ratio of 12.3. However, the standard k-ε model was more accurate at higher momentum flux ratios, and showed better agreement with experimental data when the geometrical effects of jet spacing and duct height were considered. Hale et al. [9] also used the standard and RNG k-ε models as well as a Reynolds stress model coupled with a two-layer model to achieve similar accuracies.

Non-reactive combustor analyses are another important tool in evaluating gas turbine engine performance, and both numerical and experimental characterizations of the flow fields of non-reacting combustors have been performed. Anacleto et al. [10] was able to quantify the flowfield in a water model of a Rich-burn, Quick-quench, Lean-burn (RQL) can type gas-turbine combustor. Correct total mass flow split was achieved in order to appropriately make comparisons to that of a true can type combustor flow field. The internal flow field was generated by jet impingement in a crossflow and dilution jet flow combining to produce complex three-dimensional effects at the combustor exit plane. Reynolds numbers were on the order of 10^5, similar to true combustor exits.

A non-uniform turbine inlet temperature generator was analyzed by Chana et al. [11] for a short duration transient turbine research facility. Cold fluid was injected in the endwall regions to generate radial variations and upstream turbulence rods were used to produce variations

in the circumferential direction. Vane heat transfer on the suction surface was found to be affected by the non-uniform temperature profile. Engine representative radial temperature distortion factors (RTDF), and overall temperature distortion factors (OTDF) were produced. Hot spots could be circumferentially swept in relation to nozzle guide vanes.

Vakil and Thole [12] reported measurements taken in a scaled up axial combustor simulator with two rows of dilution jets and liner wall film cooling. Dilution jet and film cooling jet momentum flux ratios and total mass flow splits were comparable with that of true combustor conditions. In addition, engine representative hole length to diameter ratios were used for the liner panels. The flow field at the combustor exit was found to be highly complex with turbulence intensity levels of near 20%. Recirculation zones entrained warm fluid in regions just downstream of the dilution jets injection. Film cooling was found to be less effective near the downstream side of the dilution holes. It is hypothesized that vortices downstream of the dilution jets are responsible for transport of film coolant flow reducing the coolants effectiveness. Stitzel and Thole [13] reported CFD simulations for the same geometry with downstream turbine interactions. Turbulence intensity at the combustor exit plane was under predicted using the RNG k-ε model. Geometry details and further characterization of the simulator used by Vakil and Thole [12] can be found in Barringer [14].

The TRF has completed the installation of the combustor simulator. This study will present preliminary CFD predictions for four typical flow conditions and four temperature variations for the TRF combustor simulator that was based on the simulator design presented in Barringer et al. [15].

EXPERIMENTAL FACILITY

The purpose of the TRF is to investigate the performance and heat transfer characteristics of full scale gas turbines. The TRF, seen in Figure 1, simulates aerothermal engine operating conditions by matching several aerodynamic and thermodynamic non-dimensional parameters such as Reynolds number, pressure ratio, corrected speed, and Mach number. The facility employs a wide array of instrumentation and data analysis techniques such as the use of total pressure and total temperature traverse mechanisms to study the high pressure vane (HPV) inlet field and exit wake region. Until presently the test rig at the TRF produced a low turbulence inlet profile that was approximately uniform in total temperature and total pressure in both the pitchwise and spanwise directions. This is in contrast to actual engine conditions where fluctuations in total temperature and pressure are prevalent as previously mentioned. It is for this reason that the combustor simulator was designed and implemented.

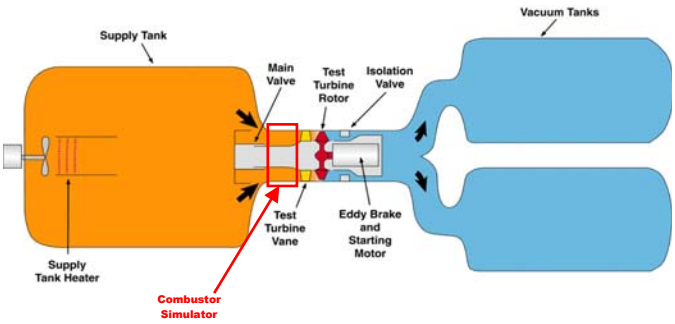

Figure 1. TRF test facility layout.

The location of the simulator in the test stand, seen in Figure 1, is between the main valve and the HPV inlet location. The non-reactive simulator with its engine representative multiple concentric annuli, seen in Figure 2a, uses two rows of staggered dilution jets to generate turbulence inside the main combustor chamber. Six rows of cooling holes on the inner diameter (ID), or hub, and outer diameter (OD), or casing, liner walls generate the high pressure and temperature gradients typically produced near the endwall regions of actual combustors. The first pitchwise row of forty four equally spaced dilution jets is centered about top dead center (TDC) of the simulator. The second pitchwise row of forty four equally spaced jets is staggered with respect to the first row. The liner wall film cooling is established by six rows of staggered holes on the ID and OD liners. The flow direction and splits can be seen in Figure 1 as the flow progresses from the supply tank through the simulator section. The core flow and first row dilution flow are highlighted in red, while the second row dilution and film cooling are shown in blue. Pressure, temperature, and velocity at the simulator exit plane will be measured at the upstream traverse rakes, located axially at X/L=1.06. Further details, including control of flow entering a particular combustor component by use of shutters, can be found in Barringer et al. [2].

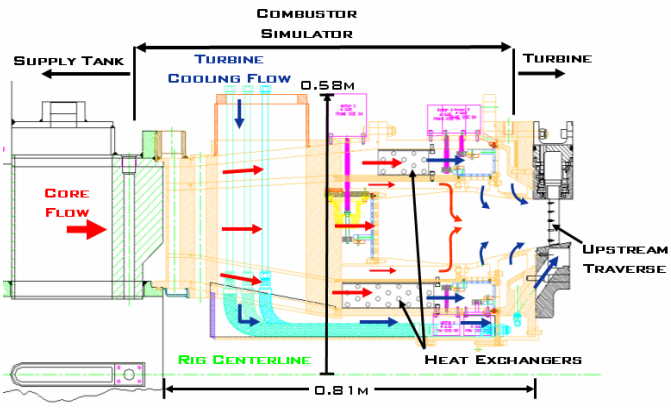

Figure 2a. Combustor simulator experimental schematic.

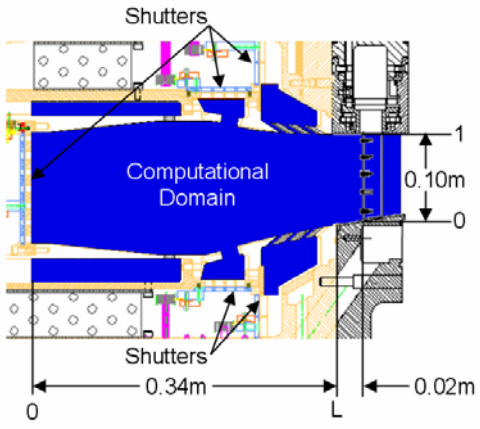

Figure 2b. Combustor simulator axial view, CFD domain.

The core flow and first row dilution jets operate at nominally the same temperature while the second row dilution flow and film cooling flow pass through a series of finned-tube heat exchangers, shown in Figure 2a, to establish desired temperature differences. The second row dilution and film cooling jets all receive flow from the same supply annulus, therefore they are restricted to operate at nominally the same temperatures, however, the temperatures on the hub and casing can be operated independently of one another.

COMPUTATIONAL MODEL

Figure 2b shows the modeled domain of the simulator beginning axially at the central chamber inlet and ending at the leading edge of the vane stage. Each of the flow inlets are modeled just after the flow control shutters. Modeling the shutters was deemed unnecessary due to the impact of the various dilution cooling flows and the axial length after the core shutter. Due to the periodicity of the forty-four dilution jets and forty-four HPV's, a 1/44th sector with periodic boundary conditions was desired to model the wetted flow paths of the simulator. Star-Design^{TM}, the solid model and grid generator, uses single degree increments for circumferentially modeling, so the 1/44th or 8.18° sector was modeled as an 8.00° or 1/45th sector. It was determined that differences in bulk flow due to the spatial difference of 0.18° would be minute and acceptable for the accuracy desired. The coolant jets proved to be a further problem as they did not divide evenly into a 1/44th sector. In a 1/44th sector the simulator has 3.3 jets on the ID side and 5.1 jets on the OD. The solid model limited locating the film cooling holes to be pitchwise spaced at 2.00° increments, allowing four film cooling jets per row for both the ID and OD sides. Consequently, if total mass flow rate through the coolant jets and true jet hole diameter to length ratios are maintained, higher coolant jet exit velocities on the OD side and lower coolant jet velocities on the ID side would occur due to the flow area difference between the CFD model and the true geometry. So, a model with altered diameter jets (larger OD jet diameter and smaller ID jet diameter) that maintained total mass flow rate and jet velocity was generated. The difference in combustor exit profiles between the two models existed only in the endwall region and was less than five percent. Therefore the model that maintained total mass flow rate and true jet hole diameter to length ratios was used. It was believed that these were the important factors to deliver the flow into the correct regions.

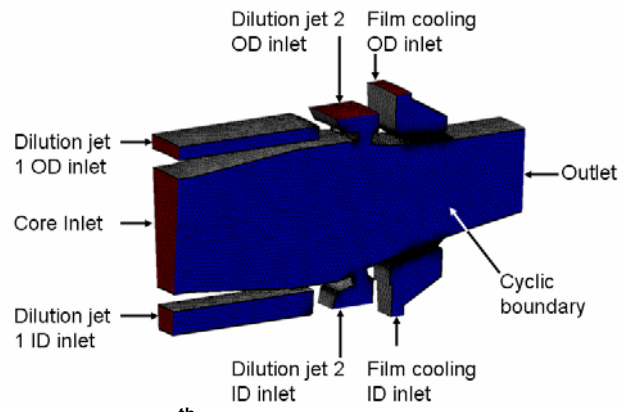

Figure 3. 1/45th meshed sector.

Star-Design^{TM} incorporates a faced based meshing technique, where the interior tetrahedron volume grid propagates from the unstructured surface mesh. The tetrahedron meshed 1/45th sector model is shown in Figure 3. The global cell size of the surface mesh dictates the grid density of the interior mesh, which can be completely unstructured or it may consist of a trimmed cell structured interior. For this analysis, the structured interior mesh was chosen to reduce the number of required cells while still maintaining accuracy of bulk fluid flow.

The model and grid file were imported into Star-CD^{TM} for secondary preprocessing and complete steady-state analysis. In addition, the geometry and grid files were split to allow parallel processing. The nature of the TRF's blow-down facility is transient. The CFD analysis is used to predict the mean exit profiles and internal flowfield, not variations with respect to time. The cyclic boundary conditions are isolated on the sides of the grid in the pitchwise directions are colored blue in Figure 3, and the fixed mass flow rate inlets are red. They impose that all scalar quantities be equal on corresponding faces [16]. The prescribed flow inlet boundary conditions specify a fixed mass flow rate where all flow must be directed inwards. The outlet boundary condition specified at the computational domain exit assumes all flow is directed outward. The distributions of values at the outlet boundary condition are extrapolated from upstream with a zero gradient assumption [16]. Density was based on ideal

gas law assumptions, and gas viscosity was calculated using the Sutherland equation. Wall boundary conditions were specified as no-slip with a standard roughness and wall heat was set at adiabatic conditions. The standard k-ε high Reynolds model was used for turbulence modeling with wall functions based on the location of accuracy desired (at the exit plane) and the success of the reviewed literature of previous studies Küpper and Henry [5], Sgarzi and Leboeuf [7], Bazdidi-Tehrani [8], and Hale et al. [9] Details of the high Reynolds model and a list of the default coefficients used in this analysis for the turbulent kinetic energy and turbulent dissipation rate equations can be found in the Star-CD™ methodology handbook [17].

Convergence is achieved using the Semi-Implicit Method for Pressure Linked Equations (SIMPLE). For numerical stability, pressure and velocity must be under-relaxed. The second order accurate Monotone Advection and Reconstruction Scheme (MARS) differencing method with a blending factor of 0.5 was used to calculate u, v, and w momentum, turbulent kinetic energy, turbulent dissipation, and temperature. Density was calculated using a second order central difference method with a blending factor of 0.01 which employs a simple linear interpolation on nearest neighbor values. Wall boundary y-plus values were monitored during the solution process and were maintained in acceptable ranges for wall functions.

A grid sensitivity analysis was conducted in order to achieve a satisfactory grid independent solution. Here a satisfactory solution indicates that the field values demonstrate no appreciable change that affects the exit profiles more than five percent with respect to grid density. Fluctuations within the simulator field values that do not affect the exit profiles appreciably are ignored and are therefore not grounds to increase grid density. Grid density is dependent on the model's global cell size and number of wall boundary extrusion layers. Global cell size is based on the mesh sizing parameter which is calculated as a percent of the total model size. A model using a global 4% relative cell size was generated first, which was then compared to a 2%, and a 1% cell size model. The 4%, 2%, and 1% cell size models consisted nominally of 400,000, 800,000, and 1,600,000 cells respectively. Y-plus values were within an acceptable wall function range (30-100) for the three models. There was approximately a fifteen percent difference in velocity magnitude at mid-span between the 4% and 2% cell size models at mid span where the solutions varied the most but there is less than two percent difference between the 2% cell size model and the 1% cell size model at mid-span, thus a 2% global cell size was sufficient to capture significant field values and give accurate combustor exit profiles.

With the global grid size established the number of extrusion layers had to be determined. The extrusion layer number is a global setting that affects all no-slip wall boundaries. Star-CD™ requires that wall boundaries be placed only on structured prismatic cells in order for turbulent wall functions to function properly for the interior tetrahedron grid. The profile shape at the combustor exit is controlled largely by the dilution jets, and the effect of extrusion layer number was found to significantly change dilution jet exit velocity profiles. Figure 4 shows this effect on the exit plane profiles for two, four, six, eight, and ten layers of prismatic near wall extrusion. There is approximately a 20% change in velocity exit profile at mid span from two to four layers, 7% change from four to six layers, 2% difference at mid span between the six and eight layer model, and less than a 1% change between eight and ten layers of wall extrusion, as seen in Figure 4. Therefore the six layer model was used for this analysis. Based on the grid sensitivity study, nominally five percent overall accuracy for this study was expected.

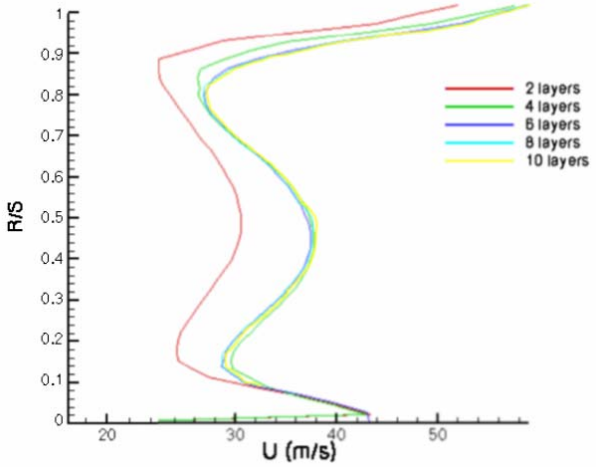

Figure 4. Exit velocity profiles at X/L=1.06.

RESULTS

The goal of the simulator was to generate total pressure and total temperature combustor exit profiles comparable to actual engines so that the performance of turbine vanes and rotors can be more accurately investigated. Four simulator configurations were modeled computationally in order to predict the simulator's ability to produce these or other engine representative profiles. The mass flow split for each of the four configurations is outlined in Table 1. Table 2 shows the corresponding momentum flux ratios (I) for each jet. The I values are determined by a ratio of the spatially averaged density and squared velocity across the jet face and the approaching crossflow density and squared velocity two jet diameters upstream from the jet injection hole. These preliminary test configurations are all operated at nominally room temperature, 300K.

Table 1. Mass flow rate rates.

Percent Total $\dot{m}$				
Inlet	Run 1	Run 2	Run 3	Run 4
D_{1OD}	8.2	16.2	14.3	11.2
D_{2OD}	13.8	28.4	25.2	17.3
FC_{OD}	11.2	6.0	19.7	11.0
Core	52.1	8.3	7.0	35.0
D_{1ID}	8.2	16.2	14.1	11.3
D_{2ID}	4.1	21.3	10.3	9.2
FC_{ID}	2.3	3.5	9.4	5.0
Total $\dot{m}$ (kg/s)	13.7	15.8	43.9	46.0

Table 2. Momentum flux ratios.

Momentum Flux Ratios				
Inlet	Run 1	Run 2	Run 3	Run 4
D_{1OD}	54.4	187.7	181.2	81.1
D_{2OD}	14.5	50.7	49.4	47.4
FC_{OD}	10.1	7.0	59.8	21.4
D_{1ID}	54.0	187.7	176.1	82.9
D_{2ID}	1.9	64.1	18.5	13.4
FC_{ID}	1.6	5.82	33.3	10.8

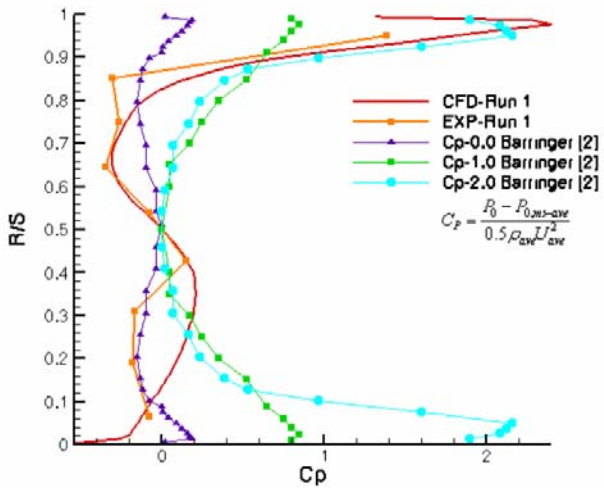

Figure 5. Pressure exit profiles experimental, CFD, and target at X/L=1.06.

The pitchwise spatially averaged CFD predicted total pressure combustor exit profile at Run 1 configuration is plotted in Figure 5. Total pressure is plotted as the non-dimensional pressure coefficient C_p. C_p which is defined as the local total pressure minus the mid-span average total pressure divided by the exit area averaged dynamic pressure. Three desired combustor exit total pressure profiles from Barringer [4] are shown in Figure 5. These profiles have a nominal C_p value of zero, one, and two at the endwall. These are the C_p values expected for this set of flow conditions. A preliminary experimental run was also performed for this case. The CFD predictions compare quite well to the experimental data. In addition, the CFD model and experimental data achieves the targeted C_p values predicting a nominal OD endwall C_p value of two and ID C_p value of zero. The benefit of the CFD model is that it predicts the entire span whereas the experimental rig obtains only discrete values and cannot measure as close to the endwall regions.

Investigation of the other three CFD cases in figure 6 reveals more of the flexibility of the simulator in generation of pressure profiles. These profiles range in casing C_p values of less than zero for the low mass flow case of Run 2 to above eight for the high mass flow Run 4 case. The ID side has lower overall mass flow rates for these cases and this is reflected in the lower endwall C_p values.

The purpose of this study is to not only predict the simulator exit profile, but to give insight into how it was generated. This will help direct experimental settings to create specific desired turbine inlet conditions. This requires studying the internal simulator flowfield in order to determine how the dilution and film cooling jets influence the exit profile. Contour plots showing normalized velocity for Run 1 are shown pitchwise at TDC in Figure 7. This plane allows the first row of dilution jets to be easily visualized. The contours have been normalized by dividing the local mean velocity value by the maximum field value. Figure 8 shows stream traces with colors corresponding to each of the inlets which aids in understanding how the exit profiles are generated as well as tracking structures in the exit plane back to their origins.

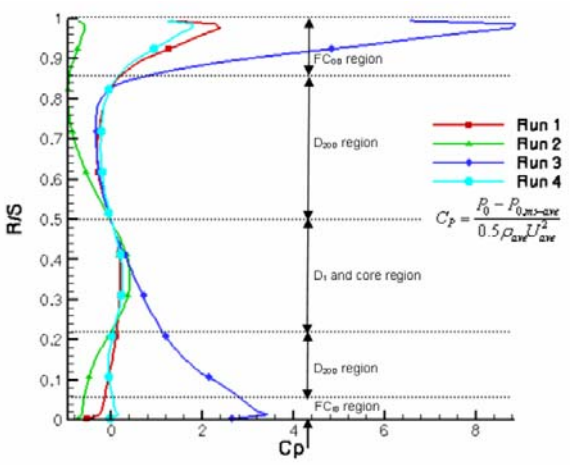

Figure 6. Computational pressure exit profiles at X/L=1.06.

Momentum flux ratios for the first row dilution jets are approximately equal causing impingement near mid-span. The jets exhibit a small amount of bending before impinging one jet diameter downstream of the injection point. This is also illustrated by the stream traces of

Figure 8 (OD jet colored red and ID jet colored cyan). A recirculation zone occurs just upstream of the impingement region and on the downstream side of the dilution jets similar to the findings of Fernandes et al. [3]. The impingement of the first row of dilution jets is the key to the generation of turbulence which will be discussed in more detail later. The two jets merge and continue downstream but are still somewhat distinct remaining relatively unmixed at the exit. The streamlines also show this to be true. The entrainment of core flow on the downstream side of the dilution jets is also apparent in Figure 8 where the core flow is recirculated.

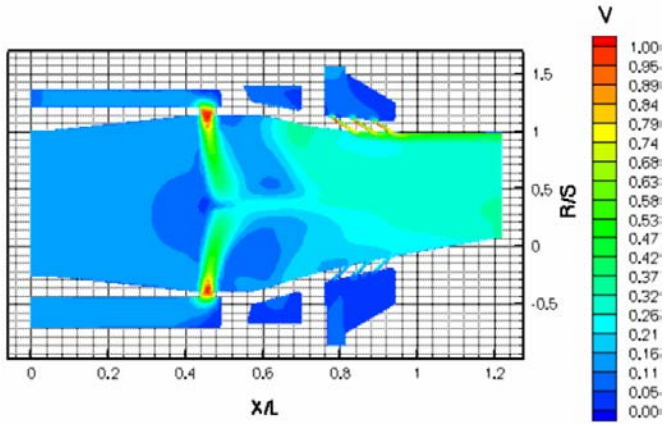

Figure 7 Run 1 normalized velocity at TDC.

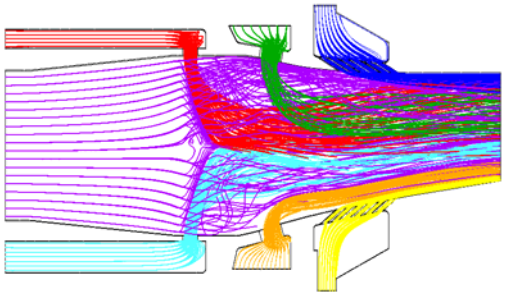

Figure 8. Run 1 stream traces.

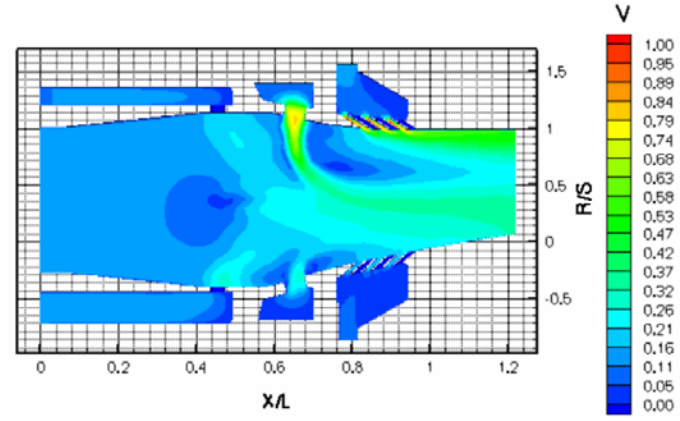

Figure 9. Run 1 velocity through dilution row two.

Figure 9 is the normalized velocity magnitude plane four degrees from TDC, through the dilution jets of row two. This plane allows visualization of the second row of dilution jets. The second row of jets are turned quickly by the core flow and do not impinge like the first row of jets. The stream traces in Figure 8 show the penetration depths more clearly. The OD (green stream traces) penetrates to mid-span, while the ID jet (orange stream traces) is confined close to the ID wall. Penetration differences are due to the difference in mass flow rate and momentum flux ratio between the two sides and are similar to the findings of Küpper and Henry [5], Morton and Ibbetson [6], and Sgarzi and Leboeuf [7]. The high penetration by the OD jets for this case actually allow the core core and first row of jets to curl under the second row of jets particularly on the ID. This results in a sheet of coolant flow immediate to the end wall. The OD spreads more due to the penetration of the second row dilution jets for this case. The film cooling is confined in the endwall regions by the core flow and second row of jets shown in Figure 8. This confinement to the endwall region is responsible for the high gradient seen in the endwall region of the exit profiles.

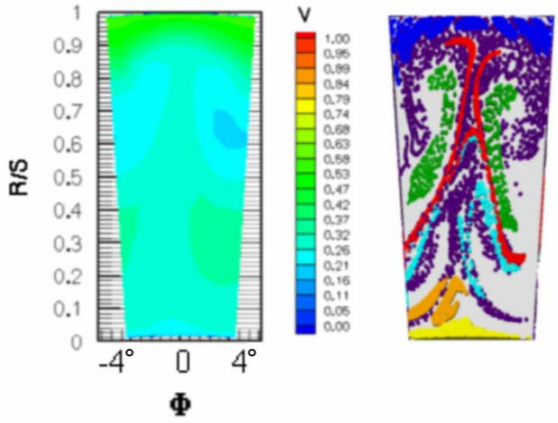

Figure 10. Run 1 velocity magnitude and streamlines at combustor exit plane

Figure 10 shows the velocity contours at the exit plane and the exit location of the streamlines for the modeled sector. Overlaying these two figures allows understanding of which flow caused the velocity gradients to occur. Streamlines leaving the domain at either periodic boundary condition can not be by calculated by Star-Design™ seen by the asymmetry and voids in stream trace distribution in Figure 10. A simplified three sector model showed that the flow does reach these voids. The influence of the dilution and film cooling jets on the exit profiles become apparent by the location of the stream traces at the exit. The first row of impinging dilution jets are circumferentially confined to a narrow region by the second row of jets (OD green stream traces and ID orange stream traces) but influence the exit profiles from approximately R/S=0.15 to R/S=0.9. The film cooling

region (blue stream trace OD side and yellow stream traces ID side) is confined by the second row of jets and the core flow. The OD film coolant jets control the exit plane from R/S=0.8 to R/S=1.0 whereas the ID only has influence from R/S=0.0 to R/S=0.02 The OD film cooling region becomes thinner at TDC indicating that the first row of jets also exerts some control of coolant distribution. In contrast, the ID film cooling region peaks at TDC indicating that the second row of ID jets influence the ID film cooling distribution, which controls the exit plan from R/S=0.0 to R/S=0.9. The ID dilution jets of row two (orange stream traces) are confined by the high momentum jets of the first row to R/S=0.05 to R/S=0.2, while the OD jets spread significantly more between R/S=0.35 to R/S=0.8. These regions of influence are also confirmed from the four computational runs in Figure 6 where the film cooling regions are apparent.

Star-CD™ calculates turbulent kinetic energy as part of the solution process, which can be used to calculate turbulence intensity. Turbulence intensity is the square root of twice the turbulent kinetic energy divided by the average exit plane velocity magnitude. Figure 11 shows the pitchwise averaged turbulence intensity exit profiles for the four runs. Vakil [12] reported similar turbulence levels for comparable flow conditions. The turbulence levels range from 10 to 45 percent for the four cases. The levels increase as the mass flow rate of the first row of jets increase. This is due to the high turbulence generation during the impingement process of those jets. Run 3 shows a significant peak at R/S=0.85. This is due to a large change in turbulent kinetic energy production at this location caused by a large change in the slope of the velocity profile. This can be seen in the C_p plot of Figure 6 for this case. Runs 1 and 4 have lesser slope changes in this region which is reflected as similar local peaks in TU. Run 2 does not exhibit this peak as the velocity profile is nearly flat in this range.

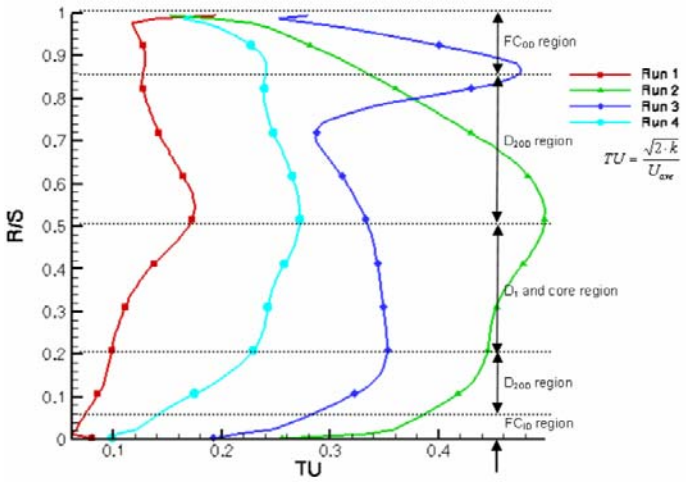

Figure 11. Turbulence intensity exit profiles at X/L=1.06.

Several test cases with variations in temperature settings have been performed using the mass flow conditions corresponding to Run 1. The tests use a constant supply temperature of 477K for the core flow and first row of dilution jets. The variations include a relative cold and warm setting for the ID (303K and 391K) and OD (303K and 400K) second row dilution and film cooling jets. The test cases show how the total temperature exit profile, shown in Figure 12, can be adjusted. These profiles are plotted utilizing the non-dimensional temperature, theta, which is calculated by subtracting the spatially averaged exit plane temperature from the cold ID and OD run and dividing by the same average.

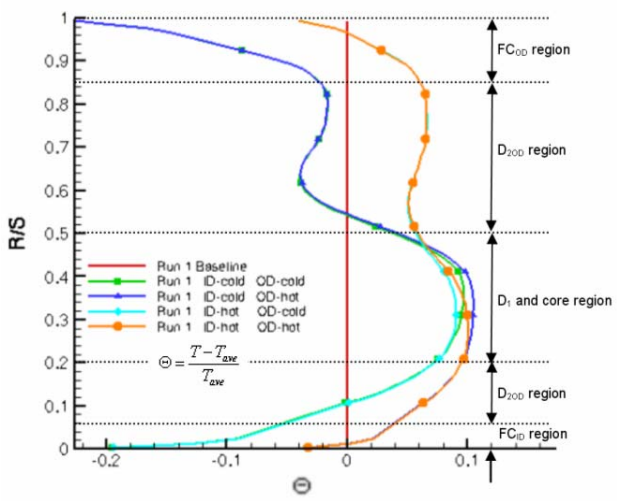

Figure 12. Temperature exit profiles at X/L=1.06.

The general shape of the profile for the warm/warm case is relatively flat in the middle 60% of the span with high temperature gradients along both endwalls as expected. Changing the temperature of the outer flow alters the profile over the entire upper half of the span. Conversely, the inner flow is only affected in the lower 25% span. Decreasing the temperature of the outer flow also results in more of a double peaked profile. This is attributed to the high momentum flux of the row two dilution jets.

Utilizing the case with the cold ID and OD settings to enhance the temperature distributions are in Figure 13, through the second row of jets, four degrees from TDC. The high mass flow rate of the OD jet results in a jet that penetrates to nearly mid-span. The spreading of this jet at the exit plane is shown in Figure 14. Here hot spots as well as cold spots are clearly visible in the circumferential and radial directions. This uneven mass flow split between the OD and ID sides coupled with the contraction on the ID side causes the total temperature exit profile at TDC to peak below mid-span. Note in both Figures 13 and 14 relatively sharp gradients. This is caused by the model under predicting the mixing of the

dilution jets also reported by Stitzel and Thole [13] using a k-ε turbulence model. However, this effect actually allows the regions of influence to be determined easier as the inlet temperatures are changed. Changing the inlet temperatures makes identification of the regions of influence easily determined.

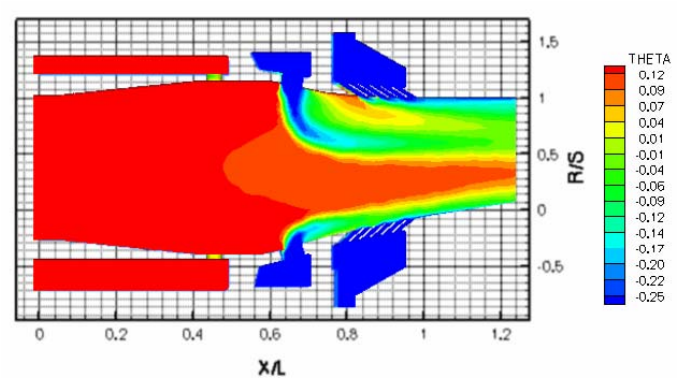

Figure 13. Total temperature through dilution row two with ID and OD annuli at cold setting

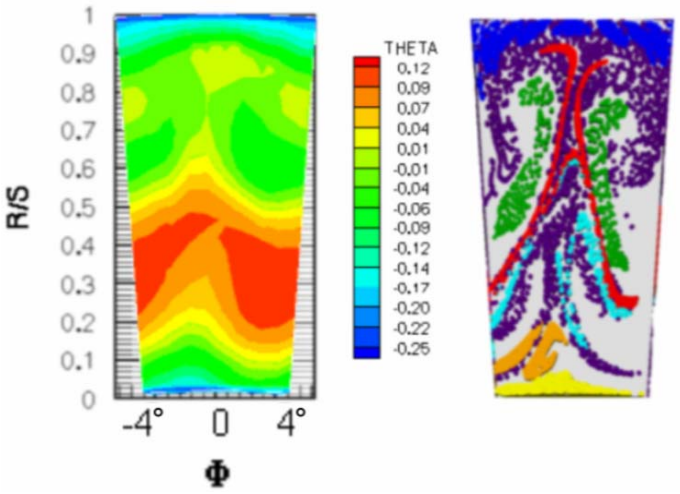

Figure 14. Total temperature at combustor exit with ID and OD annuli at cold setting

The ID film cooling jets in this configuration are confined to the region near the wall from R/S=0.0 to R/S=0.05 due to the low momentum flux ratio on the ID side. Row two ID jets control the profile from R/S=0.02 to R/S=0.2. From R/S=0.2 to R/S=0.45 the profile is relatively flat due to the hot gases from the core flow and first row of dilution jets. The OD jets of row two have significant influence R/S=0.45 and R/S=0.85, where the OD film cooling becomes the dominating influence. A second hot region exists around R/S=0.85 due to the high momentum flux ratio of the second dilution jet as indicated in the streamlines of figure 14. The core flow and first row of jets roll under the second row of dilution flow bringing hot gases close to the endwall. Figure 14 indicates where this flow is at the exit plane, which corresponds directly to the hot region of the profile. It is apparent that by altering the momentum flux of the second row of jets that the location of the primary peak in Θ can be shifted radially.

CONCLUSIONS

A three-dimensional CFD analysis of a non-reactive annular combustor simulator has been performed. Forecasts of the complex internal flow dynamics of the simulator were presented. Using Star-Design™ and Star-CD™ a 1/45th sector model of the wetted flow paths were computationally modeled. Computational results compare well with preliminary experimental findings and overall facility goals. Origins of structures in the exit plane were tracked enabling a characterization of the combustor exit profiles and pitchwise variations. This will enable tailoring of the simulator exit profile. With the CFD model, the correct amount of flow in each region can be approximately determined to set a desired pressure and temperature resultant profile. Dilution jets of row one impinge and pinch off much of the core flow creating a stagnation point and recirculation zones. This results in turbulence generation which corresponds to the momentum flux ratio of these jets. Dilution jets of row two remain relatively unmixed producing pitchwise variations in total pressure and velocity exit profiles. Row one Dilution jet flow is confined towards the middle of the exit plane and the film cooling jet flow is restrained to the ID and OD endwall regions. The CFD will help guide the experimental tasks enabling desired flow conditions to be obtained. This will allow future research to be performed investigating the effects of these profiles on vane and rotor loading and heat transfer.

ACKNOWLEDGEMENTS

The authors would like to acknowledge the support of the AFRL/PRT and the Dayton Area Graduate Studies Institute (DAGSI). In particular, AFRL contract F33615-98-C-2895, under contract monitor Dr. Charles Cross, and DAGSI project PR-UC-01-17. In addition the support of Virginia Polytechnic Institute and State University is appreciated.

REFERENCES

[1] Bicen, A., Tse, D., and Whitelaw, J., "Flow and Combustion Characteristics of an Annular Combustor," *Combustion and Flame*, Vol. 72, pp. 175-192, 1988.

[2] Barringer, M. D., Thole, K. A., and Polanka, M. D., "Developing a Combustor Simulator for Investigating High Pressure Turbine Aerodynamics and Heat Transfer," ASME Paper No. GT2004-53613, 2004.

[3] Fernandes, R. L. J., Sobiesiak, A., and Pollard, A., "Opposed Round Jets Issuing Into a small Aspect Ratio Channel Cross Flow," *Experimental Thermal and Fluid Science*, Vol. 13, pp. 374-394, 1996.

[4] Khan, Zia U. and Johnston, James P., "On Vortex Generating Jets," *Inernational Journal of Heat and Fluid Flow*, Vol. 21, pp. 506-511, 2000.

[5] Küpper, Christoph and Henry, Frank S., "Numerical Study of Air-Jet Vortex Generators in a Turbulent Boundary Layer," *Applied Mathematical Modeling*, Vol. 27, pp. 359-377, 2003.

[6] Morton, B. R. and Ibbetson, A., "Jets Deflected in a Crossflow," *Experimental Thermal and Fluid Science*, Vol. 12, pp. 112-133, 1996.

[7] Sgarzi, O., and Leboeuf, F., "Analysis of Vortices in Three-Dimensional Jets Introduced in a Cross-Flow Boundary-Layer," ASME Paper No. 97-GT-517, 1997.

[8] Bazdidi-Tehrani, F., Shahmir, A., and Haghparast-Kashani, A., "Numerical Analysis of a Single Row of Coolant Jets Injected into a Heated Crossflow," *Journal of Computational and Applied Mathematics*, Vol. 168, pp. 53-63, 2004.

[9] Bazdidi-Tehrani, Charles A., Plesniak, Michael W., and Ramadhyani, Satish, "Structural Features and Surface Heat Transfer Associated With a Row of Short-Hole Jets in Crossflow," *International Journal of Heat and Fluid Flow*, Vol. 21, pp. 542-553, 2000.

[10] Anacleto, P., Heitor, M. V., and Moreira, A. L. N., "The Mean and Turbulent Flowfields in a Model RQL Gas-Turbine Combustor," *Experiments in Fluids*, Vol. 22, pp. 153-164, 1996.

[11] Chana, Kam S., Hurrion, James R., and Jones, Terry V., "The Design, Development and Testing of a Non-Uniform Inlet Temperature Generator for the QinetiQ Transient Turbine Research Facility," ASME Paper No. GT2003-38469, 2003.

[12] Vakil, S. S., and Thole, K. A., "Flow and Thermal Field Measurements in a Combustor Simulator Relevant to a Gas Turbine Aero-Engine," ASME Paper No. GT-2003-38254, 2003.

[13] Stitzel, Sarah, and Thole, Karen A., " Flow Field Computations of Combustor-Turbine Interactions Relevant to a Gas Turbine Engine," ASME Paper No. GT2003-38253, 2003.

[14] Barringer, M. D., "Design and Benchmarking of a Combustor Simulator Relevant to Gas Turbine Engines," Master's Thesis, Virginia Polytechnic Institute and State University, 2001.

[15] Barringer, M. D., Richard, O., Stitzel, S., Walter, J., and Thole, K., 2002, "Flow Filed Simulations of a Gas Turbine Combustor," *Journal of Turbomachinery*, Vol. 124, pp. 508-516.

[16] CD Adapco Group, STAR-CD User Guide, Version 3.20. 2004.

[17] CD Adapco Group, STAR-CD Methodology, Version 3.20. 2004.